



Shaping pulses to control bistable systems: Analysis, computation and counterexamples[☆]



Aivar Sootla^a, Diego Oyarzún^b, David Angeli^{c,d}, Guy-Bart Stan^e

^a Montefiore Institute, University of Liège, B-4000, Belgium

^b Department of Mathematics, Imperial College London, UK

^c Department of Electrical and Electronic Engineering, Imperial College London, UK

^d Department of Information Engineering, University of Florence, Italy

^e Department of Bioengineering, Imperial College London, UK

ARTICLE INFO

Article history:

Received 25 February 2015

Received in revised form

27 July 2015

Accepted 5 October 2015

Available online 11 November 2015

Keywords:

Monotone systems

Near-monotone systems

Toggle switch

Control by pulses

Open-loop control

Event-based control

ABSTRACT

In this paper we study how to shape temporal pulses to switch a bistable system between its stable steady states. Our motivation for pulse-based control comes from applications in synthetic biology, where it is generally difficult to implement real-time feedback control systems due to technical limitations in sensors and actuators. We show that for monotone bistable systems, the estimation of the set of all pulses that switch the system reduces to the computation of one non-increasing curve. We provide an efficient algorithm to compute this curve and illustrate the results with a genetic bistable system commonly used in synthetic biology. We also extend these results to models with parametric uncertainty and provide a number of examples and counterexamples that demonstrate the power and limitations of the current theory. In order to show the full potential of the framework, we consider the problem of inducing oscillations in a monotone biochemical system using a combination of temporal pulses and event-based control. Our results provide an insight into the dynamics of bistable systems under external inputs and open up numerous directions for future investigation.

© 2015 Elsevier Ltd. All rights reserved.

1. Introduction

In this paper we investigate how to switch a bistable system between its two stable steady states using external input signals. Our main motivation for this problem comes from synthetic biology, which aims to engineer and control biological functions in living cells (Brophy & Voigt, 2014). Most of current research in synthetic biology focuses on building biomolecular circuits inside cells through genetic engineering. Such circuits can control cellular

functions and implement new ones, including cellular logic gates, cell-to-cell communication and light-responsive behaviours. These systems have enormous potential in diverse applications such as metabolic engineering, bioremediation, and even the energy sector (Purnick & Weiss, 2009).

Several recent works (Menolascina, Di Bernardo, & Di Bernardo, 2011; Miliás-Argeitis et al., 2011; Uhlenendorf et al., 2012) have showcased how cells can be controlled externally via computer-based feedback and actuators such as chemical inducers or light stimuli (Levskaya, Weiner, Lim, & Voigt, 2009; Mettetal, Muzzey, Gomez-Urbe, & van Oudenaarden, 2008). An important challenge in these approaches is the need for real-time measurements, which tend to be costly and difficult to implement with current technologies. In addition, because of technical limitations and the inherent nonlinearity of biochemical interactions, actuators are severely constrained in the type of input signals they can produce. As a consequence, the input signals generated by traditional feedback controllers (e.g. PID or model predictive control) may be hard to implement without a significant decrease in control performance.

In this paper we show how to switch a bistable system without the need for output measurements. We propose an open-loop

[☆] Dr. Sootla and Dr. Stan acknowledge support by the EPSRC grants EP/G036004/1, EP/J014214/1. Dr. Stan is additionally supported by the EPSRC grant EP/M002187/1. Dr. Sootla is now supported by an F.R.S.–FNRS Fellowship. Dr. Oyarzún is supported by a Junior Research Fellowship from ICL. Part of this work was performed, while Dr. Sootla was a post-doctoral research associate at ICL. The material in this paper was partially presented at the 2015 American Control Conference, July 1–3, 2015, Chicago, IL, USA. This paper was recommended for publication in revised form by Associate Editor Shun-ichi Azuma under the direction of Editor Toshiharu Sugie.

E-mail addresses: asootla@ulg.ac.be (A. Sootla), d.oyarzun@imperial.ac.uk (D. Oyarzún), d.angeli@imperial.ac.uk (D. Angeli), g.stan@imperial.ac.uk (G.-B. Stan).

control strategy based on a temporal pulse of suitable magnitude μ and duration τ :

$$u(t) = \mu h(t, \tau), \quad h(t, \tau) = \begin{cases} 1 & 0 \leq t \leq \tau, \\ 0 & t > \tau. \end{cases} \quad (1)$$

Our goal is to characterise the set of all pairs (μ, τ) that can switch the system between the stable steady states and the set of all pairs (μ, τ) that cannot. We call these sets the *switching sets* and a boundary between these sets the *switching separatrix*. The pairs (μ, τ) close to the switching separatrix are especially important in synthetic biology applications, as a large μ or a large τ can trigger toxic effects that slow down cell growth or cause cell death.

In a previous paper (Sootla, Oyarzún, Angeli, & Stan, 2015), we showed that for monotone systems the switching separatrix is a monotone curve. This result was therein extended to a class of non-monotone systems whose vector fields can be bounded by vector fields of monotone systems. This idea ultimately leads to robustness guarantees under parametric uncertainty. These results are in the spirit of Gennat and Tibken (2008); Ramdani, Meslem, and Candau (2009, 2010), where the authors considered the problem of computing reachability sets of a monotone system. Some parallels can be also drawn with Chisci and Falugi (2006); Meyer, Girard, and Witrant (2013), where feedback controllers for monotone systems were proposed.

Contributions. In the present paper we provide the first complete proof of our preliminary results in Sootla, Oyarzún, Angeli, and Stan (2015) and extend them in several directions. We formulate necessary and sufficient conditions for the existence of the monotone switching separatrix for non-monotone systems. Although it is generally hard to use this result to establish monotonicity of the switching separatrix, we use it to prove the converse. For example, we show that for a bistable Lorenz system the switching separatrix is not monotone. We then generalise the main result of Sootla et al. (2015) by providing conditions for the switching separatrix to be a graph of a function. We also discuss the relation between bifurcations and the mechanism of pulse-based switching, which provides additional insights into the switching problem. We use this intuition to show and then explain the failure of pulse-based control on an HIV viral load control problem (Adams, Banks, Kwon, & Tran, 2004). We proceed by providing a numerical algorithm to compute the switching separatrices for monotone systems. The algorithm can be efficiently distributed among several computational units and does not explicitly use the vector field of the model. We evaluate the computational tools and the theory on the bistable LacI–TetR system, which is commonly referred to as a *genetic toggle switch* (Gardner, Cantor, & Collins, 2000).

We complement our theoretical findings with several observations that illustrate limitations of the current theory and highlight the need for deeper investigations of bistable systems. For example, we show that for a toxin–antitoxin system (Cataudella, Snepfen, Gerdes, & Mitarai, 2013), the switching separatrix appears to be monotone, even though the system does not appear to be monotone. Finally, in order to demonstrate the full potential of pulse-based control, we consider the problem of inducing an oscillatory behaviour in a generalised repressilator system (Strelkova & Barahona, 2010).

Organisation. In Section 2 we cover the basics of monotone systems theory, formulate the problem in Section 2.1, and provide an intuition into the mechanism of pulse-based switching for monotone systems in Section 2.2. We also provide some motivational examples for the development of our theoretical results, which we present in Section 3. In Section 4 we derive the computational algorithm and evaluate it on the LacI–TetR system. In Section 5, we provide examples, counterexamples and an application of inducing oscillations in a generalised repressilator system. The proofs are found in the Appendix.

Notation. Let $\|\cdot\|_2$ stand for the Euclidean norm in \mathbb{R}^n , Y^* stand for a topological dual to Y , $X \setminus Y$ stand for the relative complement of X in Y , $\text{int}(Y)$ stand for the interior of the set Y , and $\text{cl}(Y)$ for its closure.

2. Preliminaries

Consider a single input control system

$$\dot{x} = f(x, u), \quad x(0) = x_0, \quad (2)$$

where $f : \mathcal{D} \times \mathcal{U} \rightarrow \mathbb{R}^n$, $u : \mathbb{R}_{\geq 0} \rightarrow \mathcal{U}$, $\mathcal{D} \subset \mathbb{R}^n$, $\mathcal{U} \subset \mathbb{R}$ and $u(\cdot)$ belongs to the space \mathcal{U}_∞ of Lebesgue measurable functions with values from \mathcal{U} . We say that the system is *unforced*, if $u = 0$. We define the *flow map* $\phi_f : \mathbb{R} \times \mathcal{D} \times \mathcal{U}_\infty \rightarrow \mathbb{R}^n$, where $\phi_f(t, x_0, u)$ is a solution to the system (2) with an initial condition x_0 and a control signal u . We consider the control signals in the shape of a *pulse*, that is signals defined in (1) with nonnegative μ and τ .

In order to avoid confusion, we reserve the notation $f(x, u)$ for the vector field of non-monotone systems, while systems

$$\dot{x} = g(x, u), \quad x(0) = x_0, \quad (3)$$

$$\dot{x} = r(x, u), \quad x(0) = x_0, \quad (4)$$

denote so-called *monotone systems* throughout the paper. In short, monotone systems preserve a partial order relation in initial conditions and input signals. A relation \succeq_x is called a *partial order* if it is reflexive ($x \succeq_x x$), transitive ($x \succeq_x y, y \succeq_x z$ implies $x \succeq_x z$), and antisymmetric ($x \succeq_x y, y \succeq_x x$ implies $x = y$). We define a partial order through a cone $K \subset \mathbb{R}^n$ as follows: $x \succeq_x y$ if and only if $x - y \in K$. We write $x \not\succeq_x y$, if the relation $x \succeq_x y$ does not hold; $x \succ_x y$, if $x \succeq_x y$ and $x \neq y$; and $x \gg_x y$, if $x - y \in \text{int}(K)$. Similarly we define a partial order on the space of signals $u \in \mathcal{U}_\infty$: $u \succeq_u v$, if $u(t) - v(t) \in K$ for all $t \geq 0$. We write $u \succ_u v$, if $u \succeq_u v$ and $u(t) \neq v(t)$ for all $t \geq 0$. Finally, a set M is called *p-convex* if for all x, y in M such that $x \succeq_x y$, and all $\lambda \in (0, 1)$ we have that $\lambda x + (1 - \lambda)y \in M$.

Definition 1. The system (3) is called *monotone* on $\mathcal{D}_M \times \mathcal{U}_\infty$ with respect to the partial orders \succeq_x, \succeq_u , if for all $x, y \in \mathcal{D}_M$ and $u, v \in \mathcal{U}_\infty$ such that $x \succeq_x y$ and $u \succeq_u v$, we have $\phi_g(t, x, u) \succeq_x \phi_g(t, y, v)$ for all $t \geq 0$. If additionally, $x \succ_x y$, or $u \succ_u v$ implies that $\phi_g(t, x, u) \gg_x \phi_g(t, y, v)$ for all $t > 0$, then the system is called *strongly monotone*.

In general, it is hard to verify monotonicity of a system with respect to an order other than an order induced by an orthant (e.g., positive orthant $\mathbb{R}_{\geq 0}^n$). Hence throughout the paper, by a monotone system we actually mean a *monotone system with respect to a partial order induced by an orthant*. A certificate for monotonicity with respect to an orthant is referred to as Kamke–Müller conditions (Angeli & Sontag, 2003).

Proposition 2 (Angeli & Sontag, 2003). Consider the system (3), where g is differentiable in x and u and let the sets $\mathcal{D}_M, \mathcal{U}$ be *p-convex*. Let the partial orders \succeq_x, \succeq_u be induced by $P_x \mathbb{R}_{\geq 0}^n, P_u \mathbb{R}_{\geq 0}^m$, respectively, where $P_x = \text{diag}((-1)^{\varepsilon_1}, \dots, (-1)^{\varepsilon_n}), P_u = \text{diag}((-1)^{\delta_1}, \dots, (-1)^{\delta_m})$ for some ε_i, δ_i in $\{0, 1\}$. Then

$$(-1)^{\varepsilon_i + \varepsilon_j} \frac{\partial g_i}{\partial x_j} \geq 0, \quad \forall i \neq j, \quad (x, u) \in \text{cl}(\mathcal{D}_M) \times \mathcal{U}$$

$$(-1)^{\varepsilon_i + \delta_j} \frac{\partial g_i}{\partial u_j} \geq 0, \quad \forall i, j, \quad (x, u) \in \mathcal{D}_M \times \mathcal{U}$$

if and only if the system (3) is monotone on $\mathcal{D}_M \times \mathcal{U}_\infty$ with respect to \succeq_x, \succeq_u .

If we consider the orthants $\mathbb{R}_{\geq 0}^n, \mathbb{R}_{\geq 0}^m$, then the conditions above are equivalent to checking if for all $x \preceq_x y$ such that $x_i = y_i$ for some i , and all $u \preceq_u v$ we have $g_i(x, u) \leq g_i(y, v)$.

2.1. Problem formulation

We confine the class of considered control systems by making the following **assumptions**:

- A1. Let $f(x, u)$ in (2) be continuous in (x, u) on $\mathcal{D}_f \times \mathcal{U}$. Moreover, for each compact sets $C_1 \subset \mathcal{D}_f$ and $C_2 \subset \mathcal{U}$, let there exist a constant k such that $\|f(\xi, u) - f(\zeta, u)\|_2 \leq k\|\xi - \zeta\|_2$ for all $\xi, \zeta \in C_1$ and $u \in C_2$;
- A2. Let the unforced system (2) have two stable steady states in \mathcal{D}_f , denoted as s_f^0 and s_f^1 ;
- A3. Let $\mathcal{D}_f = \text{cl}(\mathcal{A}(s_f^0) \cup \mathcal{A}(s_f^1))$, where $\mathcal{A}(s_f^i)$ stands for the domain of attraction of the steady state s_f^i for $i = 0, 1$ of the unforced system (2);
- A4. For any $u = \mu h(\cdot, \tau)$ with finite μ and τ let $\phi_f(t, s_f^0, u)$ belong to $\text{int}(\mathcal{D}_f)$. Moreover, let the sets

$$\mathcal{S}_f^+ = \left\{ \mu, \tau > 0 \mid \lim_{t \rightarrow \infty} \phi_f(t, s_f^0, \mu h(\cdot, \tau)) = s_f^1 \right\}$$

$$\mathcal{S}_f^- = \left\{ \mu, \tau > 0 \mid \lim_{t \rightarrow \infty} \phi_f(t, s_f^0, \mu h(\cdot, \tau)) = s_f^0 \right\}$$

be non-empty.

Assumption A1 guarantees existence, uniqueness and continuity of solutions to (2), while Assumptions A2–A3 define a bistable system on a set \mathcal{D}_f controlled by pulses. In Assumption A4 we define the *switching sets*: the set \mathcal{S}_f^+ , which contains all (μ, τ) pairs that switch the system, and the set \mathcal{S}_f^- , which contains all pairs that do not. The boundary between these sets is called the *switching separatrix*. In the rest of the paper, we focus on the **control problem** of estimating the switching sets.

2.2. Mechanism of pulse-based switching

The general problem of switching a bistable system with external inputs is amenable to an optimal control formulation. However, in applications such as synthetic biology, optimal control solutions can be very hard to implement due to technical limitations in sensors and actuators. Additionally, the solution of this optimal control problem may be technically challenging. Hence applying open-loop pulses can be a reasonable solution, if we can guarantee some form of robustness. As we shall see later, our results show that for monotone systems, pulse-based switching is computationally tractable and robust towards parameter variations.

Before presenting our main results, we first provide an intuitive link between monotonicity and the ability to switch a system with temporal pulses. If we consider constant inputs $u = \mu$ and regard μ as a bifurcation parameter, we have the following result with the proof in the [Appendix](#).

Proposition 3. *Let the system (3) satisfy Assumptions A1–A4 and be monotone on $\mathcal{D}_g \times \mathcal{U}_\infty$ with respect to $\mathbb{R}_{\geq 0}^n, \mathbb{R}_{\geq 0}$. Let μ_{\min} be such that all pairs $(\mu, \tau) \in \mathcal{S}_g^-$ for $0 < \mu < \mu_{\min}$, and any finite positive τ . Let also $\xi(\mu) = \lim_{t \rightarrow \infty} \phi_g(t, s_g^0, \mu)$ and $\eta(\mu) = \lim_{t \rightarrow \infty} \phi_g(t, s_g^1, \mu)$. Then*

- (1) If $\mu \leq \lambda < \mu_{\min}$ then $\xi(\mu) \preceq_x \xi(\lambda)$, $\eta(\mu) \preceq_x \eta(\lambda)$;
- (2) If $0 < \mu < \mu_{\min}$ then $\xi(\mu) \in \mathcal{A}(s_g^0)$ and $\xi(\mu) \prec_x \eta(\mu)$;
- (3) The function $\xi(\mu)$ is discontinuous at μ_{\min} .

In many applications, the functions $\xi(\mu), \eta(\mu)$ are simply evolutions of the steady states s_g^0, s_g^1 with respect to the parameter μ , respectively. Hence, statement (1) of [Proposition 3](#) shows how the steady states move with respect to changes in μ . Statement (2) ensures that there are at least two distinct asymptotically stable equilibria for $\mu < \mu_{\min}$. Finally, statement (3) indicates that the system undergoes a bifurcation for $\mu = \mu_{\min}$. The particular type of the bifurcation will depend on a specific model. Next we investigate further aspects of this result with some examples of monotone and non-monotone bistable systems.

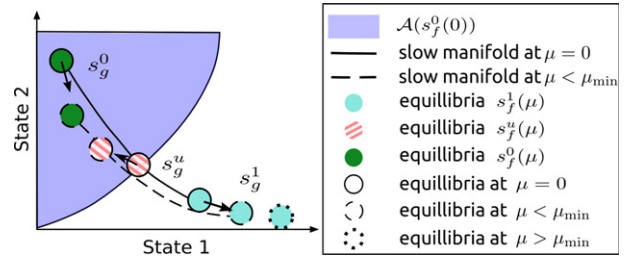


Fig. 1. A schematic depiction of the evolution of the stable nodes $s_g^0(\mu), s_g^1(\mu)$ and the saddle $s_g^u(\mu)$ with respect to μ in the genetic toggle switch system. By slow manifold we mean a manifold connecting stable equilibria and a saddle. The arrows show the direction of the equilibria movements with increasing μ . Note that $s_g^0(\mu), s_g^u(\mu)$ are increasing in the order induced by $\text{diag}\{1, -1\}\mathbb{R}_{\geq 0}^2$. At μ_{\min} the equilibria $s_g^0(\mu)$ and $s_g^u(\mu)$ collide resulting in a saddle–node bifurcation preserving only $s_g^1(\mu)$.

Example 1 (LacI–TetR Switch.). The genetic system composed of two mutually repressive genes *LacI* and *TetR* is typically called the genetic toggle switch and was a pioneering system for synthetic biology ([Gardner et al., 2000](#)). Presently, toggle switches are widely used in synthetic biology to trigger cellular functions in response to extracellular signals ([Brophy & Voigt, 2014](#); [Khalil & Collins, 2010](#)). We consider its control-affine model, which is consistent with a toggle switch actuated by light induction ([Levskaya et al., 2009](#)):

$$\begin{aligned} \dot{x}_1 &= \frac{p_1}{1 + (x_2/p_2)^{p_3}} + p_4 - p_5 x_1 + u, \\ \dot{x}_2 &= \frac{p_6}{1 + (x_1/p_7)^{p_8}} + p_9 - p_{10} x_2, \end{aligned} \quad (5)$$

where x_i represents the concentration of each protein, whose mutual repression is modelled via a rational function. The parameters p_2 and p_7 represent the repression thresholds, whereas p_4 and p_9 model the basal synthesis rate of each protein. The parameters p_5 and p_{10} are the degradation rate constants, p_1, p_6 describe the strength of mutual repression, and p_3, p_8 are called Hill (or cooperativity) parameters. By means of [Proposition 2](#) we can readily check that the model is monotone on $\mathbb{R}_{\geq 0}^2 \times \mathbb{R}_{\geq 0}$ for all nonnegative parameter values with respect to the orders induced by $\text{diag}\{1, -1\}\mathbb{R}_{\geq 0}^2 \times \mathbb{R}_{\geq 0}$. It can be verified by direct computation that the system satisfies Assumptions A1–A4 with $\mathcal{D}_f = \mathbb{R}_{\geq 0}^2$. We chose the following values of parameters

$$\begin{aligned} p_1 &= 40, & p_2 &= 1, & p_3 &= 4, & p_4 &= 0.05, \\ p_5 &= 1, \\ p_6 &= 30, & p_7 &= 1, & p_8 &= 4, & p_9 &= 0.1, \\ p_{10} &= 1, \end{aligned} \quad (6)$$

and numerically found a bifurcation to occur at $\mu_{\min} \approx 1.4077$. For $\mu < \mu_{\min}$ the system has two stable nodes and a saddle. We observe that $\xi(\mu) = \eta(\mu)$ for all $\mu > \mu_{\min}$, and therefore we conclude that the system undergoes a saddle–node bifurcation, as illustrated in [Fig. 1](#).

Example 2 (Lorenz System). Consider a system

$$\begin{aligned} \dot{x}_1 &= \sigma(x_2 - x_1) + u \\ \dot{x}_2 &= x_1(\rho - x_3) - x_2 + u \\ \dot{x}_3 &= x_1 x_2 - \beta x_3 \end{aligned}$$

with parameters $\sigma = 10, \rho = 21, \beta = 8/3$, which is non-monotone and bistable with two stable foci. Numerical computation of the sets \mathcal{S}^- and \mathcal{S}^+ in [Fig. 2](#) suggests that the switching separatrix is not monotone. We will revisit this conclusion in the next section using our theoretical results.

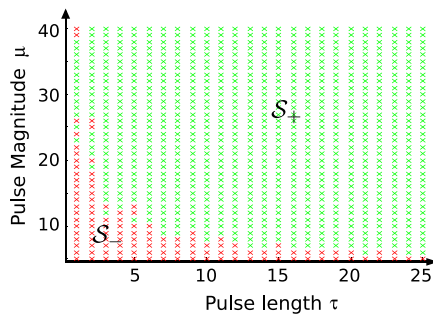


Fig. 2. Switching sets for the Lorenz system. We simulated the Lorenz system for (μ, τ) pairs taken from a mesh grid. The green and red crosses correspond to the pairs that switched or not switched the system, respectively. (For interpretation of the references to colour in this figure legend, the reader is referred to the web version of this article.)

Example 3 (HIV Viral Load Control Problem). In Adams et al. (2004) the authors considered the problem of switching from a “non-healthy” (s^0) to a “healthy” (s^1) steady state by means of control inputs u_1 and u_2 that model different drug therapies. Due to space limitations we refer the reader to (Adams et al., 2004) for a description of the model. It can be verified that both steady states are stable foci and that the model is not monotone. Although the system can be switched with non-pulse control signals (Adams et al., 2004), using extensive simulations we were unable to find a combination of pulses in u_1 and u_2 switching the system.

As in the case of a monotone bistable system, we found a bifurcation with respect to constant control signals $u_1 = \mu_1$ and $u_2 = \mu_2$. More specifically, we fixed $\mu_2 = 0.4$, and numerically found a bifurcation at $\mu_1 \approx 0.7059$. The major difference between this case and the monotone system case (Example 1) is that the steady state $s^1(0.7059, 0.4)$ lies the domain of attraction of $s^0(0, 0)$. Hence if we stop applying the constant control signal we regress back to the initial point $s^0(0, 0)$. Furthermore, with increasing μ_1 the steady state $s^1(\mu_1, 0.4)$ is moving towards the origin, which also lies in the domain of attraction of $s^0(0, 0)$. This makes pulse-based switching very difficult, if not impossible.

3. Theoretical results

In Sootla et al. (2015) we showed that the switching separatrix of a monotone bistable system $\dot{x} = g(x, u)$ is non-increasing. Here we present a generalisation of this result by formulating necessary and sufficient conditions for the switching separatrix to be monotone, the proof of which is found in the Appendix.

Theorem 4. Let the system (2) satisfy Assumptions A1–A4. Then the following properties are equivalent:

- (1) If $\phi_f(t, s_f^0, \bar{\mu}h(\cdot, \bar{\tau}))$ belongs to $\mathcal{A}(s_f^0)$ for all $t \geq 0$, then $\phi_f(t, s_f^0, \mu h(\cdot, \tau))$ belongs to $\mathcal{A}(s_f^0)$ for all $t \geq 0$, and for all μ, τ such that $0 < \mu \leq \bar{\mu}, 0 < \tau \leq \bar{\tau}$.
- (2) The set \mathcal{S}_f^- is simply connected. There exists a curve $\mu_f(\tau)$, which is a set of maximal elements of \mathcal{S}_f^- in the standard partial order. Moreover, the curve $\mu_f(\tau)$ is such that for any $\mu_1 \in \mu_f(\tau_1)$ and $\mu_2 \in \mu_f(\tau_2), \mu_1 \geq \mu_2$ for $\tau_1 < \tau_2$.

Theorem 4 shows that the computation of the set \mathcal{S}_f^- is reduced to the computation of a curve $\mu_f(\tau)$. This result also provides a connection between the geometry of domains of attraction of the unforced system and the switching separatrix. As shown next, Theorem 4 can also be used to establish non-monotonicity of the switching separatrix.

Remark 5 (Lorenz System Revisited). Consider the Lorenz system from the previous section and three different pulses $u_i(t) = \mu_i h(t, \tau)$ with $\mu_1 = 24, \mu_2 = 25, \mu_3 = 26$, and $\tau = 1$. Numerical solutions show that the flows $\phi(t, s^0, u_1)$ and $\phi(t, s^0, u_3)$ converge to s^0 , whereas $\phi(t, s^0, u_2)$ converges to s^1 . Application of Theorem 4 proves that the switching separatrix is not monotone.

The major bottleneck in the direct application of Theorem 4 is the verification of condition (1), which is generally computationally intractable. For example, condition (1) is satisfied if the partial order is preserved for control signals. That is for any $u \leq v$, it should follow that $\phi_g(t, s_g^0, u) \leq_x \phi_g(t, s_g^0, v)$ for all $t > 0$. Although this property is weaker than monotonicity, it is not clear how to verify it. Monotonicity, on the other hand, is easy to check and implies condition (1) in Theorem 4. This is used in the following result.

Theorem 6. Let the system (3) satisfy Assumptions A1–A4 and be monotone on $\mathcal{D}_g \times \mathcal{U}_\infty$. Then:

- (1) The set \mathcal{S}_g^- is simply connected. There exists a curve $\mu_g(\tau)$, which is a set of maximal elements of \mathcal{S}_g^- in the standard partial order. Moreover, the curve $\mu_g(\tau)$ is such that for any $\mu_1 \in \mu_g(\tau_1)$ and $\mu_2 \in \mu_g(\tau_2), \mu_1 \geq \mu_2$ for $\tau_1 < \tau_2$.
- (2) The set \mathcal{S}_g^+ is simply connected. There exists a curve $\nu_g(\tau)$, which is a set of minimal elements of \mathcal{S}_g^+ in the standard partial order. Moreover, the curve $\nu_g(\tau)$ is such that for any $\nu_1 \in \nu_g(\tau_1)$ and $\nu_2 \in \nu_g(\tau_2), \nu_1 \geq \nu_2$ for $\tau_1 < \tau_2$.
- (3) Let the system (3) be strongly monotone and $\partial\mathcal{A}$ be the separatrix between the domains of attractions $\mathcal{A}(s_f^0)$ and $\mathcal{A}(s_f^1)$ of the unforced system (3). Let additionally $\partial\mathcal{A}$ be an unordered manifold, that is, there are no x, y in $\partial\mathcal{A}$ such that $x >_x y$. Then $\nu_g(\tau) = \mu_g(\tau)$ for all $\tau > 0$ and the curve $\mu_g(\cdot) = \nu_g(\cdot)$ is a graph of a monotonically decreasing function.

We note that our computational procedure (see Section 4) does not require that $\mu_g(\tau) = \nu_g(\tau)$ or that $\mu_g(\cdot), \nu_g(\cdot)$ are graphs of functions. Hence we treat point (3) in Theorem 6 as a strictly theoretical result, but remark that sufficient conditions for the separatrix $\partial\mathcal{A}$ to be unordered are provided in Jiang, Liang, and Zhao (2004, Theorem 2.1). The most relevant condition to our case is that the unforced system is strongly monotone, which we also assume in Theorem 6.

Besides $\mu_g(\tau) \neq \nu_g(\tau)$, there are other pathological cases. For example, applying constant input control signals $u = \mu$ typically results in a system (2) with a different set of steady states than s_f^0 or s_f^1 . Moreover, the number of equilibria may be different. Hence, with $\tau \rightarrow \infty$ the set \mathcal{S}_f^+ typically does not contain the limiting control signal $u = \mu$. If the set of pairs (μ, τ) resulting in these pathological cases is not measure zero, then the sets $\text{cl}(\mathcal{S}_f^+)$ and $\text{cl}(\mathbb{R}_{\geq 0}^2 \setminus \mathcal{S}_f^-)$ are not equal, which can complicate the computation of the switching sets. However, in many applications, the sets $\text{cl}(\mathcal{S}_f^+)$ and $\text{cl}(\mathbb{R}_{\geq 0}^2 \setminus \mathcal{S}_f^-)$ appear to be equal. Therefore in order to simplify the presentation we study only the properties of \mathcal{S}_f^- .

If the system $\dot{x} = f(x, u)$ is not monotone, then the curve $\mu_f(\tau)$ may not be monotone, which is essential for our computational procedure. Instead, we estimate inner and outer bounds on the switching set provided that the vector field of the system can be bounded from above and below by vector fields of monotone systems. This is formally stated in the next result with the proof in the Appendix.

Theorem 7. Let systems (2), (3), (4) satisfy Assumptions A1–A4. Let $\mathcal{D}_M = \mathcal{D}_g \cup \mathcal{D}_f \cup \mathcal{D}_r$, the systems (3) and (4) be monotone on $\mathcal{D}_M \times \mathcal{U}_\infty$ and

$$g(x, u) \leq_x f(x, u) \leq_x r(x, u) \quad \text{on } \mathcal{D}_M \times \mathcal{U}. \quad (7)$$

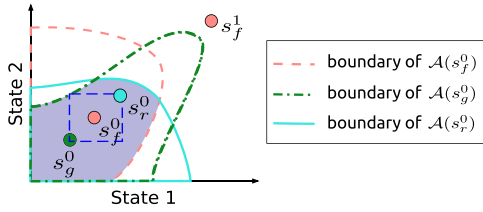


Fig. 3. A schematic depiction of conditions (8) and (9). Condition (8) ensures that all the steady states lie in the intersection of the corresponding domains of attractions (violet area). The steady state s_f^1 cannot lie in the dashed blue box due to (9). (For interpretation of the references to colour in this figure legend, the reader is referred to the web version of this article.)

Assume that the stable steady states $s_g^0, s_f^0, s_r^0, s_f^1$ satisfy

$$s_g^0, s_f^0, s_r^0 \in \text{int}(\mathcal{A}(s_g^0) \cap \mathcal{A}(s_f^0) \cap \mathcal{A}(s_r^0)), \quad (8)$$

$$s_f^1 \notin \{z | s_g^0 \leq_x z \leq_x s_r^0\}. \quad (9)$$

Then the following relations hold:

$$\mathcal{S}_g^- \supseteq \mathcal{S}_f^- \supseteq \mathcal{S}_r^-. \quad (10)$$

The technical conditions in (8), (9) (which are illustrated in Fig. 3) are crucial to the proof and are generally easy to satisfy. Verifying the condition (9) reduces to the computation of the stable steady states, as does checking the condition (8). Indeed, to ensure that s_f^0 belongs to the intersection of $\mathcal{A}(s_g^0), \mathcal{A}(s_f^0), \mathcal{A}(s_r^0)$, we check if the trajectories of the systems (3), (4) initialised at s_f^0 with $u = 0$ converge to s_g^0 and s_r^0 , respectively, which is done by numerical integration of differential equations. The computation of stable steady states can be done using the methods from Zwolak, Tyson, and Watson (2004).

In some applications, we need to find a subset of the pairs (μ, τ) that switch the system (2) from s_f^0 to s_f^1 . Due to the inclusion $\mathcal{S}_g^- \supseteq \mathcal{S}_f^-$, existence of the system (3) allows to do that. In this case, we are only interested in finding the system (3), hence the condition (9) is not required and the condition (8) is transformed to $s_g^0, s_f^0 \in \text{int}(\mathcal{A}(s_g^0) \cap \mathcal{A}(s_f^0))$.

Remark 8. The proofs of Theorems 6 and 7 are adapted in a straightforward manner to the case when systems are monotone with respect to orders \succeq_x, \succeq_u induced by an arbitrary cone K_x and $\mathbb{R}_{\geq 0}$, respectively. In examples, however, we always assume that K_x is an orthant.

Theorem 7 also provides a way of estimating the switching set under parametric uncertainty, which is stated in the next corollary.

Corollary 9. Consider a family of systems $\dot{x} = f(x, u, p)$ with a vector of parameters p taking values from a compact set \mathcal{P} . Let the systems $\dot{x} = f(x, u, p)$ satisfy Assumptions A1–A4 for every p in \mathcal{P} . Assume there exist parameter values a, b in \mathcal{P} such that the systems $\dot{x} = f(x, u, a)$ and $\dot{x} = f(x, u, b)$ are monotone on $\mathcal{D}_M \times \mathcal{U}_\infty$, where $\mathcal{D}_M = \bigcup_{q \in \mathcal{P}} \mathcal{D}_{f(\cdot, \cdot, q)}$ and

$$f(x, u, a) \leq_x f(x, u, p) \leq_x f(x, u, b), \quad (11)$$

for all $(x, u, p) \in \mathcal{D}_M \times \mathcal{U} \times \mathcal{P}$. Let also

$$s_{f(\cdot, \cdot, p)}^0 \in \text{int}\left(\bigcap_{q \in \mathcal{P}} \mathcal{A}(s_{f(\cdot, \cdot, q)}^0)\right), \quad (12)$$

$$s_{f(\cdot, \cdot, p)}^1 \notin \{z | s_{f(\cdot, \cdot, a)}^0 \leq_x z \leq_x s_{f(\cdot, \cdot, b)}^0\}, \quad (13)$$

for all p in \mathcal{P} . Then the following relations hold:

$$\mathcal{S}_{f(\cdot, \cdot, a)}^- \supseteq \mathcal{S}_{f(\cdot, \cdot, p)}^- \supseteq \mathcal{S}_{f(\cdot, \cdot, b)}^- \quad \forall p \in \mathcal{P}. \quad (14)$$

The proof follows by setting $g(x, u) = f(x, u, a)$ and $r(x, u) = f(x, u, b)$ and noting that the conditions in (12), (13) imply the conditions in (8), (9) in the premise of Theorem 7.

Theorem 7 states that if the bounding systems (3), (4) can be found, the switching sets $\mathcal{S}_g^-, \mathcal{S}_r^-$ can be estimated, thereby providing approximations on the switching set \mathcal{S}_f^- . Here we provide a procedure to find monotone bounding systems if the system (2) is near-monotone, meaning that by removing some interactions between the states the system becomes monotone (see Sontag, 2007 for the discussion on near-monotone systems). Let there exist a single interaction which is not compatible with monotonicity with respect to an order induced by $\mathbb{R}_{\geq 0}^n$. Namely, let the (i, j) -th entry in the Jacobian $\frac{\partial f_i}{\partial x_j}$ be smaller than zero. A monotone system can be obtained by replacing the variable x_j with a constant in the function $f_i(x, u)$, which removes the interaction between the states x_i and x_j . If the set \mathcal{D} is bounded then clearly we can find \bar{x}_j and \underline{x}_j such that $\bar{x}_j \geq x_j \geq \underline{x}_j$ for all $x \in \mathcal{D}$. If the set \mathcal{D} is not bounded, then we need to estimate the bounds on the intersection of $\mathcal{A}(s_f^0)$ and the reachability set starting at s_f^0 for all admissible pulses. Let $g_k = r_k = f_k$ for all $k \neq i$, $g_i(x, u) = f_i(x, u)|_{x_j=\bar{x}_j}$, and $r_i(x, u) = f_i(x, u)|_{x_j=\underline{x}_j}$. It is straightforward to show that $\dot{x} = g(x, u)$, and $\dot{x} = r(x, u)$ are monotone systems and their vector fields are bounding the vector field f from below and above, respectively. Note that in order to apply Theorem 7 we still need to check if these bounding systems satisfy Assumptions A1–A4.

In the case of Corollary 9, the procedure is quite similar. If the system $\dot{x} = f(x, u, p)$ is monotone for all parameter values p , then we can find a, b if there exists a partial order in the parameter space. That is a relation \leq_p such that for parameter values p_1 and p_2 satisfying $p_1 \leq_p p_2$ we have that

$$f(x, u, p_1) \leq_x f(x, u, p_2) \quad \forall x \in \mathcal{D}, u \in \mathcal{U}.$$

If a partial order is found, the values a and b are computed as minimal and maximal elements of \mathcal{P} in the partial order \leq_p . This idea is equivalent to treating parameters p as inputs and showing that the system $\dot{x} = f(x, u, p)$ is monotone with respect to inputs u and p .

4. Computation of the switching separatrix

The theoretical results in Section 3 guarantee the existence of the switching separatrix for monotone systems, but in order to compute $\mu(\tau)$ we resort to numerical algorithms.

Given a pair (μ, τ) we can check if this pair is switching the system using numerical integration. If the curve $\mu(\tau)$ is a monotone function, then for every τ there exists a unique pulse magnitude $\mu = \mu(\tau)$. Let $\mathcal{T} = \{\tau_i\}_{i=1}^N$ be such that $\tau_{\min} = \tau_1 \leq \tau_i \leq \tau_{i+1} \leq \tau_N = \tau_{\max}$ for all i . Clearly, for every τ_i we can compute the corresponding μ_i using bisection. We start the algorithm by computing the value μ_1 corresponding to τ_1 . Due to monotonicity of the switching separatrix, the minimal switching magnitude μ_2 for the pulse length τ_2 is smaller or equal to μ_1 . Therefore, we can save some computational effort by setting the upper bound on the computation of μ_2 equal to μ_1 . The computation of the pairs (μ, τ) can be parallelised by setting the same upper bound on $\mu_i, \dots, \mu_{i+N_{\text{par}}}$, where N_{par} is the number of independent computations. As an output we obtain \mathcal{M}_{\min} and \mathcal{M}_{\max} , which are the sets of pairs (μ, τ) approximating the switching separatrix from below and above, respectively.

In order to evaluate the error of computing the switching separatrix consider Fig. 4. According to the definitions in the caption of Fig. 4 we define the relative error of the approximation as

$$E_{\text{rel}} = (\mu_{\text{err}}/(\mu_{\max} - \mu_{\min}) + \tau_{\text{err}}/(\tau_{\max} - \tau_{\min}))/2.$$

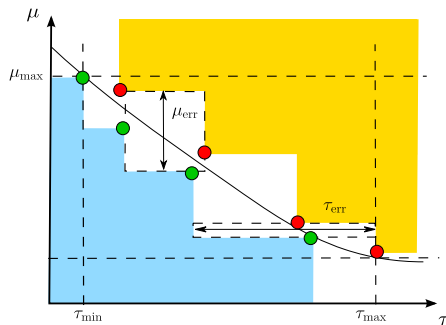


Fig. 4. Illustration of the error of computation of the switching separatrix between the values τ_{\min} , τ_{\max} . The black curve is the switching separatrix to be computed, the red and green circles are the upper and lower bounding points, respectively. The switching separatrix should lie between the coloured regions due to its monotonicity. The values μ_{err} and τ_{err} are the largest height and width of boxes inscribed between the coloured regions, respectively. (For interpretation of the references to colour in this figure legend, the reader is referred to the web version of this article.)

Note that, even if the green and red circles lie very close to each other the relative error can be substantial. In numerical simulations we use a logarithmic grid for τ , which yields a significantly lower relative error in comparison with an equidistant grid. This can be explained by an observation that in many numerical examples $\mu(\tau)$ appears to be an exponentially decreasing curve.

There are a few drawbacks in the bisection algorithm. Firstly, it requires a large number of samples. Secondly, the choice of the grid is not automatic, which implies that for switching separatrices with different geometry the relative error on the same grid may be drastically different. Finally, the algorithm relies on the assumption that $\mu(\tau)$ is a graph of a monotone function, which may not be true. In order to overcome these difficulties, we have derived Algorithm 1 based on random sampling, which converges faster than the bisection algorithm, has higher sample efficiency, does not require a predefined grid and the graph assumption. Some of the steps in Algorithm 1 require additional explanation:

Step 7. Find two boxes: the box \mathcal{B}_μ with the maximal height (denoted as μ_{err}) and the box \mathcal{B}_τ with the maximal width (denoted as τ_{err}) that can be inscribed between the coloured regions as depicted in Fig. 4.

Step 9. Generate N_ε samples of τ using a probability distribution δ between τ_{\min} and τ_{\max} . For every τ generate a value μ using a distribution δ such that μ lies in the area between the coloured regions. Repeat this step by first generating μ between μ_{\min} and μ_{\max} using a distribution δ , and then generating τ for every generated μ in the area between the coloured regions.

Step 13. First, we update the sets \mathcal{M}^{\min} , \mathcal{M}^{\max} by adding the samples that do not switch and switch the system, respectively. Now if there exist two pairs (μ_1, τ_1) and (μ_2, τ_2) in the set \mathcal{M}^{\min} (resp., \mathcal{M}^{\max}) such that $\mu_1 \leq \mu_2$ and $\tau_1 \leq \tau_2$, then delete the pair (μ_1, τ_1) from the set \mathcal{M}^{\min} (resp., the pair (μ_2, τ_2) from the set \mathcal{M}^{\max}).

Note that Step 11 is the most computationally expensive part of the algorithm and its computation is distributed into N_{par} independent tasks. In our implementation, we chose δ as a Beta distribution with parameters 1 and 3, and adjusted the support to a specific interval. Note that the set between the coloured regions is getting smaller with every generated sample, hence the relative error of Algorithm 1 is a non-increasing function of the total number of samples. In fact, numerical experiments show that this function is on average exponentially decreasing. After the sets \mathcal{M}^{\min} and \mathcal{M}^{\max} are generated one can employ machine learning algorithms to build a closed form approximation of the switching separatrix (e.g., Sparse Bayesian Learning Tipping, 2001; see also Pan, Sootla, & Stan, 2014, Wipf et al., 2008 for efficient algorithms).

Algorithm 1 Computation of Switching Separatrix Based on Random Sampling

- 1: **Inputs:** The system $\dot{x} = f(x, u)$ with initial state s_f^0 , final state s_f^1 , total number of samples N , simulation time t_e , lower and upper bounds on τ , τ_{\min} and τ_{\max} respectively, the numbers N_{gr} , N_ε , probability distribution δ
- 2: **Outputs:** sets \mathcal{M}^{\min} and \mathcal{M}^{\max}
- 3: Compute μ_{\min} and μ_{\max} using bisection for values τ_{\min} and τ_{\max}
- 4: Set $\mathcal{M}^{\max} = \mathcal{M}^{\min} = \{(\mu_{\max}, \tau_{\min}), (\mu_{\min}, \tau_{\max})\}$
- 5: Set $N_{\text{par}} = 2(N_{\text{gr}} + N_\varepsilon)$
- 6: **for** $i = 1, \dots, [N/N_{\text{par}}]$ **do**
- 7: Compute the values μ_{err} , τ_{err} , and the corresponding boxes \mathcal{B}_μ , \mathcal{B}_τ .
- 8: Generate N_{gr} samples (μ, τ) in each of the boxes \mathcal{B}_μ and \mathcal{B}_τ using a probability distribution δ
- 9: Generate randomly $2N_\varepsilon$ samples
- 10: **for** $j = 1, \dots, N_{\text{par}}$ **do**
- 11: Check if the samples (μ, τ) switch the system
- 12: **end for**
- 13: Update and prune the sets \mathcal{M}^{\min} , \mathcal{M}^{\max}
- 14: **end for**

Evaluation of the Computational Algorithm. Here we compare the bisection algorithm and Algorithm 1 with different parameter values, as well as their distributed implementations on the LaCl-TetR switch introduced in Section 2.2. Note that Algorithm 1 does not depend explicitly on the dynamics of the underlying system. Therefore, the convergence and sample efficiency results presented here will be valid for a broad class of systems. In Fig. 5, we compare the error against the total number of generated samples. Since checking if a sample switches the system or not is the most expensive part of both algorithms, the total number of samples reflects the computational complexity. In the case of Algorithm 1 with $N_\varepsilon = 0$ the randomisation level is not high, hence an average over ten runs is sufficient to demonstrate the average behaviour of this algorithm. Note that Algorithm 1 with $N_\varepsilon = 0$ outperforms the bisection algorithm in the centralised and parallelised settings.

Some computational effort in Algorithm 1 goes into computing the error. However, this effort appears to be negligible in comparison with numerically solving a differential equation for a given pair (μ, τ) even for such a small system as the toggle switch. We run the simulations on a computer equipped with Intel Core i7-4500U processor and 8 GB of RAM. Using the centralised version of Algorithm 1 we achieved on average a relative error equal to 0.0448 in 87.65 s, while it took 89.17 s to obtain a relative error equal to 0.0842 with the bisection algorithm. For systems with a larger number of states the difference may be larger.

In Fig. 5, we also compare the sample efficiency of the algorithms, which we define as

$$N_{\text{eff}} = |\mathcal{M}^{\min} \cup \mathcal{M}^{\max}|/N,$$

where N is the total number of generated samples, and $|\mathcal{M}^{\min} \cup \mathcal{M}^{\max}|$ is the number of samples in the set $\mathcal{M}^{\min} \cup \mathcal{M}^{\max}$. Results in Fig. 5 indicate that Algorithm 1 has higher sample efficiency than the bisection algorithm.

Our results also indicate that Algorithm 1 with $N_{\text{gr}} = 5$, $N_\varepsilon = 5$ has on average a higher empirical convergence rate and a higher sample efficiency than Algorithm 1 with $N_{\text{gr}} = 10$, $N_\varepsilon = 0$. This indicates that a combination of non-zero N_{gr} , N_ε improves convergence and sample efficiency, which can be explained as follows. When the total number of generated samples is low, we do not have sufficient information on the behaviour of the switching separatrix. Therefore we need to explore this behaviour by randomly generating samples, before we start minimising the relative error. This idea is similar to the so-called exploration/exploitation trade-off in reinforcement learning (Buşoniu, Babuška, De Schutter, & Ernst, 2010).

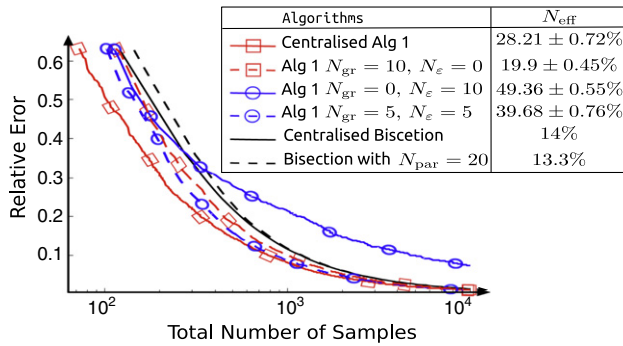


Fig. 5. Average error against total number of generated samples. The curves corresponding to the bisection algorithm are computed by a single run of the algorithm. The curves corresponding to $N_e = 0$ are averages over ten runs of Algorithm 1, while the curves for $N_e > 0$ are the averages over twenty runs of Algorithm 1. Recall that $N_{\text{par}} = 2(N_{\text{gr}} + N_e)$ for Algorithm 1. In the table we list sample efficiency N_{eff} in percent. In the notation $x \pm y$, x, y stand for the empirical mean, standard deviation, respectively.

5. Examples, counterexamples and applications

Robust Switching in the LacI–TetR System introduced in Section 2.2. We specify a system $\mathcal{F}_{\text{upper}}$ with $p_1 = 40, p_4 = 0.05, p_6 = 30, p_9 = 0.1$ and a system $\mathcal{F}_{\text{lower}}$ with $p_1 = 20, p_4 = 0.01, p_6 = 45, p_9 = 0.3$. The remaining parameters are the same as in (6). After that we compute the switching separatrices and plot them in Fig. 6. According to Corollary 9, the system with parameter values $p_1 \in [20, 40], p_4 \in [0.01, 0.005], p_6 \in [30, 65], p_9 \in [0.1, 0.3]$ and the remaining parameters as in (6) will have the switching separatrix lying between the solid and dashed green curves in Fig. 6. If other parameters are varied then the bounds on the separatrices may be looser as discussed in Sootla et al. (2015). Therein we also illustrate the application of Theorem 7 to a perturbed non-monotone LacI–TetR switch.

Toxin–Antitoxin System describes interaction between the toxin proteins T and antitoxin proteins A (Cataudella et al., 2013):

$$\begin{aligned} \dot{T} &= \frac{\sigma_T}{\left(1 + \frac{[A_f][T_f]}{K_0}\right) (1 + \beta_M [T_f])} - \frac{1}{(1 + \beta_C [T_f])} T, \\ \dot{A} &= \frac{\sigma_A}{\left(1 + \frac{[A_f][T_f]}{K_0}\right) (1 + \beta_M [T_f])} - \Gamma_A A + u, \\ \varepsilon \dot{[A_f]} &= A - \left([A_f] + \frac{[A_f][T_f]}{K_T} + \frac{[A_f][T_f]^2}{K_T K_{TT}}\right), \\ \varepsilon \dot{[T_f]} &= T - \left([T_f] + \frac{[A_f][T_f]}{K_T} + 2 \frac{[A_f][T_f]^2}{K_T K_{TT}}\right), \end{aligned}$$

where $[A_f], [T_f]$ is the number of free toxin and antitoxin proteins. In Cataudella et al. (2013), the authors considered the model with $\varepsilon = 0$, but in order to simplify our analysis we set $\varepsilon = 10^{-6}$. If the parameters are chosen as follows: $\sigma_T = 166.28, K_0 = 1, \beta_M = \beta_C = 0.16, \sigma_A = 10^2, \Gamma_A = 0.2, K_T = K_{TT} = 0.3$, then the system is bistable with two stable nodes. But the system is not monotone and we were not able to find bounding systems satisfying Assumptions A1–A4. Nevertheless, we estimated the switching separatrix on a mesh grid and noticed that the switching separatrix appears to be monotone. We can provide some intuition behind this phenomenon. With ε tending to zero, we can apply singular perturbation theory (cf. Khalil, 2002) to eliminate the states $[A_f], [T_f]$. Numerical computations indicate that the reduced order system is not monotone in $\mathbb{R}_{\geq 0}^2$, however, it is monotone around the stable equilibria, which may explain monotonicity of the switching separatrix.

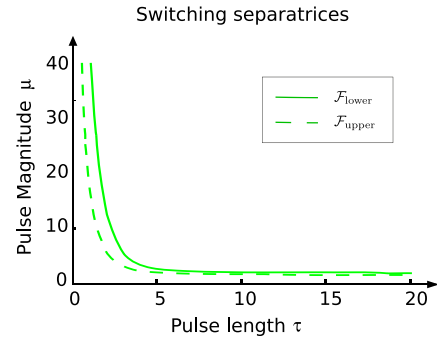


Fig. 6. Switching separatrices for the LacI–TetR system (5).

Switching in a Mass Action Kinetics System from Wilhelm (2009):

$$\begin{aligned} \dot{x}_1 &= f_1(x_1, x_2) = 2k_1 x_2 - k_2 x_1^2 - k_3 x_1 x_2 - k_4 x_1 + \beta u, \\ \dot{x}_2 &= f_2(x_1, x_2) = k_2 x_1^2 - k_1 x_2. \end{aligned}$$

Without loss of generality we assume that $k_2 = 1$, since we can remove one of the parameters using a simple change of variables. Let $L = k_1 - 4k_3 k_4$, if $L > 0$ then the unforced system is bistable with stable nodes s^0, s^1 and a saddle s^u :

$$\begin{aligned} s^0 &= \begin{pmatrix} 0 \\ 0 \end{pmatrix} & s^u &= \begin{pmatrix} \frac{k_1 - \sqrt{k_1 L}}{2k_3} \\ \left(\frac{\sqrt{k_1} - \sqrt{L}}{2k_3}\right)^2 \end{pmatrix} \\ s^1 &= \begin{pmatrix} \frac{k_1 + \sqrt{k_1 L}}{2k_3} \\ \left(\frac{\sqrt{k_1} + \sqrt{L}}{2k_3}\right)^2 \end{pmatrix}. \end{aligned}$$

It can be verified that the system is monotone on $\mathcal{D} = \{x_1, x_2 | 0 \leq x_1 \leq 2k_1/k_3\}$, which also contains the equilibria and hence the system satisfies our assumptions.

The derivatives of f_1, f_2 with respect to k_1 do not have the same sign hence the system is not monotone with respect to parameter k_1 . This term appears due to so-called mass action kinetics, which are common in biological applications and hence this problem is met often. A straightforward solution is to treat every instance of k_1 as an independent parameter. Hence we have a vector of parameters $[k_{11}, k_3, k_4, k_{12}]$, where k_{11} is the instance of k_1 entering the first equation, and k_{12} is the instance of k_1 entering the second equation. Let $k_1 \in [7.7, 8.3], k_3 \in [1, 1.2], k_4 \in [1, 1.2]$ and consider the lower bounding parameter vector $p_l = [7.7, 1.2, 1.2, 8.3]$, and the upper bounding parameter vector $p_u = [8.3, 1, 1, 7.7]$. We apply Corollary 9 only to relatively small perturbations in parameters, since with larger variations the system becomes mono- or unstable. There is no indication that this problem is unique to this system, and does not appear in other mass-action systems.

We conclude this example by performing a sweep for the parameter $k_1 \in [6, 10]$, while $k_2 = k_3 = 1$. Numerical simulations suggest that for any $k_1 \in (6, 10)$ the switching separatrix appears to lie between the switching separatrices for $k_1 = 6$ and $k_1 = 10$, respectively. Again we can only provide some intuition behind this observation. It is straightforward to verify that the gradient of s^u with respect to k_1 is a negative vector, and the gradient of s^1 with respect to k_1 is a positive vector. Hence the equilibria depend on k_1 in the way which is consistent with a behaviour of a monotone system. This example indicates that the behaviour of the equilibria may be one of the necessary conditions allowing the switching separatrix to be a monotone curve and change monotonically with respect to parameter variations.

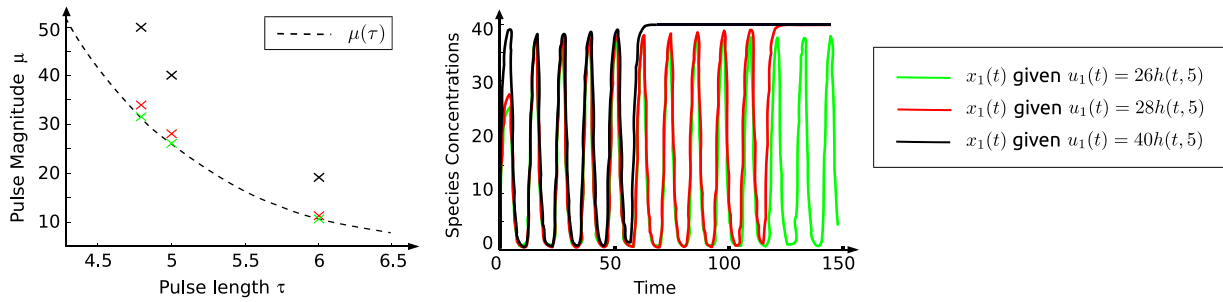


Fig. 7. Switching between steady states in a generalised repressilator system. All trajectories generated by the pairs (μ, τ) corresponding to the black crosses in the left panel will converge to a steady state with the same rate as the black curve in the right panel. Similar correspondence is valid for the red and green crosses in the left panel and the red and green curves in the right panel. This observation indicates that the closer the pair (μ, τ) is to the switching separatrix the longer oscillations will persist. (For interpretation of the references to colour in this figure legend, the reader is referred to the web version of this article.)

Shaping Pulses to Induce Oscillations in an Eight Species Generalised Repressilator. An eight species generalised repressilator is an academic example, where each of the species represses another species in a ring topology. The corresponding dynamic equations for a symmetric generalised repressilator are as follows:

$$\begin{aligned} \dot{x}_1 &= \frac{p_1}{1 + (x_8/p_2)^{p_3}} + p_4 - p_5x_1 + u_1, \\ \dot{x}_2 &= \frac{p_1}{1 + (x_1/p_2)^{p_3}} + p_4 - p_5x_2 + u_2, \\ \dot{x}_i &= \frac{p_1}{1 + (x_{i-1}/p_2)^{p_3}} + p_4 - p_5x_i, \quad \forall i = 3, \dots, 8, \end{aligned} \quad (15)$$

where $p_1 = 40, p_2 = 1, p_3 = 3, p_4 = 0.5,$ and $p_5 = 1.$ This system has two stable nodes s^1 and s^2 and is monotone with the respect to $P_x \mathbb{R}^8 \times P_u \mathbb{R}^2,$ where $P_x = \text{diag}([1, -1, 1, -1, 1, -1, 1, -1]),$ $P_u = \text{diag}([1, -1]).$ The control signal u_1 can switch the system from the state s^1 to the state $s^2,$ while the control signal u_2 can switch the system from the state s^2 to the state $s^1.$ The switching separatrix for the control signal u_1 is depicted in the left panel of Fig. 7. Note that the separatrix is identical for the control signal $u_2,$ since the repressilator is symmetric.

Numerical simulations suggest that the trajectories exhibit an oscillatory behaviour, while switching between the stable steady states using a pulse. This is in agreement with previous studies that showed the existence of unstable periodic orbits (Strelkova & Barahona, 2010) in a generalised repressilator. Switching trajectories of species x_1 for various pairs (μ, τ) are depicted in the right panel of Fig. 7. The observations made in the caption of Fig. 7 indicate that the closer the pair (μ, τ) is to the switching separatrix the longer oscillations will persist.

We can set up another control problem: *to induce oscillations in the generalised repressilator.* One can address the problem by forcing the trajectories to be close to the unstable periodic orbit of the system, which, however, is very hard to compute. In Sootla, Strelkova, Ernst, Barahona, and Stan (2013), it was proposed to track other periodic trajectories instead. However, the solution was very computationally expensive and offering little insight into the problem. Here we will use pulses to induce oscillations as was proposed in Strelkova and Barahona (2010). In contrast to (Strelkova & Barahona, 2010), we provide a way to shape all possible pulses inducing oscillations.

Let the initial point be $s^1.$ We can shape the control signal u_1 to switch to the state $s^2.$ Once we have reached an ε -ball around the state $s^2,$ we can shape the control signal u_2 to switch back to the state s^1 and so on. During switching we will observe oscillations depending on the position of the pair (μ, τ) with respect to the switching separatrix. Now we need to define an automatic way of switching between the steady states. Let \mathcal{M}_ε be equal to $\{z | s^1 + \varepsilon P_x \mathbf{1} \preceq_x z \preceq_x s^2 - \varepsilon P_x \mathbf{1}\},$ where $\mathbf{1}$ is the vector of ones and $\varepsilon > 0.$

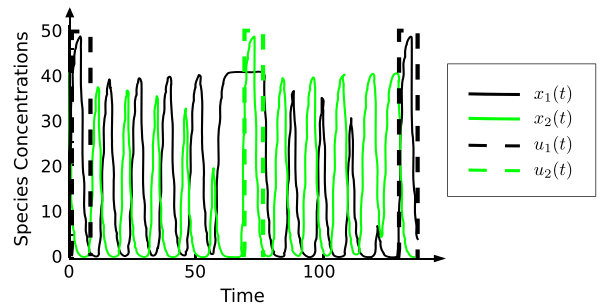


Fig. 8. Inducing oscillatory behaviour in the generalised repressilator system with eight species. The pulses for both u_1 and u_2 are equal, and are generated using a pair $(\mu, \tau) = (48, 4.8).$ The pair $(48, 4.8)$ lies relatively far from the switching separatrix, hence the time between switches is not large.

It can be verified that the trajectories observed in Fig. 7 lie in \mathcal{M}_ε for a small enough ε due to monotonicity. Since the repressilator is symmetric we can assume that the shape of pulses for both u_1 and u_2 is the same and formalise our control strategy as follows. If the event $x(t_e) \preceq_x s^1 + \varepsilon P_x \mathbf{1}$ occurs at time $t_e,$ then

$$u_1(\cdot) = \mu h(\cdot, t_e + \tau) \quad u_2(\cdot) = 0.$$

If the event $x(t_e) \succeq_x s^2 - \varepsilon P_x \mathbf{1}$ occurs at time $t_e,$ then

$$u_1(\cdot) = 0 \quad u_2(\cdot) = \mu h(\cdot, t_e + \tau).$$

Note that we change the entire control signals when the event occurs at some time $t_e.$ Due to this fact, the pulse $\mu h(\cdot, t_e + \tau)$ is of length $\tau.$ The resulting trajectories for the species x_1 and $x_2,$ as well as control signals are depicted in Fig. 8. Our control algorithm falls into the class of event-based control, with the events occurring if $x(t_e)$ leaves $\mathcal{M}_\varepsilon.$ For a small enough $\varepsilon,$ our control strategy induces oscillations.

6. Conclusion and discussion

In this paper we have presented a framework for shaping pulses to control bistable systems. Our main motivation comes from control problems arising in Synthetic Biology, but the results hold in other classes of bistable systems. We considered the problem of switching between stable steady states using temporal pulses. We showed that the problem is feasible, if the flow of the controlled system can be bounded from above and below by flows of monotone systems. We presented a detailed analysis of the conditions needed for switching, together with an algorithm to compute the pulse's length and duration. We illustrated the theory with a number of case studies and counterexamples that shed light on the limitations of the approach and highlight the need for further theoretical tools to control bistable non-monotone systems.

Throughout this work we did not take into account stochasticity in the model dynamics, which can be particularly important in biochemical systems (Elowitz, Levine, Siggia, & Swain, 2002). Noisy bistable dynamics can be controlled, for example, using reinforcement learning algorithms as the ones described in Sootla et al. (2013); Sootla, Strelkowa, Ernst, Barahona, and Stan (2014). These approaches, however, require large amounts of measurement data that are typically impractical to acquire. A promising extension to our results is the switching problem in stochastic bimodal systems. This requires the use of the so-called stochastically monotone Markov decision processes, for which a whole new set of theoretical tools needs to be developed. Work in this direction started in Sootla (2015) and the references within, addressing the extension of the concept of monotonicity to stochastic systems.

Acknowledgement

The authors would like to thank Dr. Alexandre Mauroy for valuable suggestions and discussions.

Appendix. Proofs

Proof of Proposition 3. (1) Here we simply need to notice that by monotonicity with $t \rightarrow \infty$ we have

$$\xi(\mu) \leftarrow \phi_g(t, s_g^0, \mu) \preceq_x \phi_g(t, s_g^0, \lambda) \rightarrow \xi(\lambda).$$

Similarly we can show that $\eta(\mu) \preceq_x \eta(\lambda)$.

(2) First, we need to show that $\xi(\mu) \in \mathcal{A}(s_g^0)$ for all $0 < \mu < \mu_{\min}$. This is straightforward, since due to the definition of μ_{\min} the flow $\phi_g(t, s_g^0, \mu h(\cdot, \tau))$ converges to s_g^0 for all the pairs $(\mu, \tau) \in \mathcal{S}^-$ for $0 < \mu < \mu_{\min}$. Hence the limit $\lim_{t \rightarrow \infty} \phi_g(t, s_g^0, \mu)$ belongs to $\mathcal{A}(s_g^0)$.

Now, we show that $s_g^0 \prec_x s_g^1$. Consider $u = 0$ and $v = \lambda h(\cdot, \tau)$ such that $(\lambda, \tau) \in \mathcal{S}^+$. Therefore we have

$$s_g^0 = \phi_g(t, s_g^0, u) \preceq_x \phi_g(t, s_g^0, v) \rightarrow s_g^1,$$

with $t \rightarrow \infty$. Since s_g^0 is not equal to s_g^1 , we have $s_g^0 \prec_x s_g^1$. Now the claim $\xi(\mu) \prec_x \eta(\mu)$ for all $0 < \mu < \mu_{\min}$ follows by monotonicity.

(3) Consider $\mu = \mu_{\min} + \varepsilon$ and τ large enough such that the pair $(\mu, \tau) \in \mathcal{S}^+$. Hence the flow $\phi_g(t, s_g^0, \mu h(\cdot, \tau))$ converges to s_g^1 . By monotonicity we have that $\phi_g(t, s_g^0, \mu) \preceq_x \phi_g(t, s_g^0, \mu h(\cdot, \tau))$, which implies that $\xi(\mu) \preceq_x s_g^1$ for arbitrarily small $\varepsilon > 0$. Since $\xi(\mu_{\min} - \varepsilon)$ lies in $\mathcal{A}(s_g^0)$ we have that $\|\xi(\mu_{\min} - \varepsilon) - \xi(\mu)\|_2 > 0$, which proves the claim.

Proof of Theorem 4. (1) \Rightarrow (2) A. It is straightforward to verify that the premise of Theorem 4 implies that any point lying in the set \mathcal{S}_f^- is path-wise connected to a point in the neighbourhood of the origin. In order to show that the set is simply connected, it is left to prove that there are no holes in the set \mathcal{S}_f^- . Let $\eta(\mu, \tau)$ be a closed curve which lies in \mathcal{S}_f^- . Consider the set

$$\mathcal{S}^\eta = \{(\mu, \tau) \mid 0 < \mu \leq \mu^\eta, 0 < \tau \leq \tau^\eta, (\mu^\eta, \tau^\eta) \in \eta(\mu, \tau)\}.$$

Since the set \mathcal{S}_f^- is in $\mathbb{R}_{>0}^2$, the set \mathcal{S}^η contains the set enclosed by the curve $\eta(\mu, \tau)$. It is straightforward to show that \mathcal{S}^η is a subset of \mathcal{S}_f^- by the premise of the theorem. Hence there are no holes in the area enclosed by the arbitrary curve $\eta \in \mathcal{S}_f^-$. Since the curve η is in \mathbb{R}^2 we can shrink this curve continuously to a point, which belongs to the set \mathcal{S}_f^- . Since the curve is an arbitrary closed curve in \mathcal{S}_f^- , the set \mathcal{S}_f^- is simply connected.

B. Let us show here that there exists a set of maximal elements in \mathcal{S}_f^- . Let a pair (μ^u, τ^u) not belong to \mathcal{S}_f^- . If there exists a pair

$(\mu, \tau) \in \mathcal{S}_f^-$ such that $\mu \geq \mu^u, \tau \geq \tau^u$, then by the arguments above the pair (μ^u, τ^u) must also belong to \mathcal{S}_f^- . Hence, all pairs (μ, τ) such that $\mu \geq \mu^u, \tau \geq \tau^u$ do not belong to \mathcal{S}_f^- . This implies that there exists a set of maximal elements of \mathcal{S}_f^- in the standard partial order, which is a segment of the boundary of \mathcal{S}_f^- excluding the points with μ and τ equal to zero.

C. It is left to establish that the set of maximal elements is unordered. Let the mapping $\mu_f(\tau)$ denote the set of maximal elements of \mathcal{S}_f^- and let $\tau_1 < \tau_2$. Since the mapping $\mu_f(\tau)$ are the maximal elements in \mathcal{S}_f^- , we cannot have $\mu_f(\tau_1) < \mu_f(\tau_2)$. Hence, $\mu_f(\tau_1) \geq \mu_f(\tau_2)$, for all $\tau_1 < \tau_2$.

(2) \Rightarrow (1) The claim follows directly from the fact that there exists a set of maximal elements $\mu_f(\tau)$ in the simply connected set \mathcal{S}_f^- .

Proof of Theorem 6. (1) Due to Assumption A4, there exists at least one point (μ^l, τ^l) in \mathcal{S}_g^- . Let us show that if a pair (μ^l, τ^l) belongs to \mathcal{S}_g^- , then all pairs (μ, τ) such that $0 < \mu \leq \mu^l, 0 < \tau \leq \tau^l$ also belong to \mathcal{S}_g^- . By the definition of the order in u , for every $0 < \mu \leq \mu^l, 0 < \tau \leq \tau^l$ we have $0 \preceq_u \mu h(t, \tau) \preceq_u \mu^l h(t, \tau^l)$. The following then holds

$$s_g^0 \preceq_x \phi_g(t, s_g^0, \mu h(\cdot, \tau)) \preceq_x \phi_g(t, s_g^0, \mu^l h(\cdot, \tau^l)).$$

By assumption, there exists a T such that for all $t > T$ the flow $\phi_g(t, s_g^0, \mu^l h(\cdot, \tau^l))$ belongs to $\mathcal{A}(s_g^0)$ and converges to s_g^0 . Therefore $\phi_g(t, s_g^0, \mu h(\cdot, \tau))$ converges to s_g^0 with $t \rightarrow +\infty$, and consequently the pair (μ, τ) does not toggle the system and thus belongs to \mathcal{S}_g^- . Therefore, by Theorem 4 $\mu_g(\tau_1) \geq \mu_g(\tau_2)$, for all $\tau_1 < \tau_2$.

(2) Due to Assumption A4, there exists at least one point (μ^l, τ^l) in \mathcal{S}_g^+ . Similarly to point (1) above, we can show that, if a pair (μ^l, τ^l) belongs to \mathcal{S}_g^+ , then by continuity of solutions to (3) there exist $\bar{\varepsilon} > 0, \bar{\delta} > 0$ such that the pairs $(\mu + \varepsilon, \tau + \delta)$ also belong to \mathcal{S}_g^+ for all $0 < \varepsilon < \bar{\varepsilon}, 0 < \delta < \bar{\delta}$. Hence the set \mathcal{S}_g^+ has a non-empty interior. The rest of the proof is the same as the proof of the implication (1) \Rightarrow (2) in Theorem 4.

(3) We prove the result by contradiction. Let there exist a τ and an interval $I = (\mu_1, \mu_2)$ such that for all $\mu \in I$ the flow $\phi_g(t, s_g^0, \mu h(\cdot, \tau))$ does not converge to s_g^0 or s_g^1 , but belongs to the interior of \mathcal{D}_g . This means that the flow $\phi_g(t, s_g^0, \mu h(\cdot, \tau))$ evolves on the separatrix $\partial \mathcal{A}$ between domains of attraction $\mathcal{A}(s_g^0)$ and $\mathcal{A}(s_g^1)$ for all $t > \tau$. Let μ_1, μ_2 belong to I and $\mu_1 < \mu_2$, which implies that $\phi_g(t, s_g^0, \mu_1 h(\cdot, \tau)) \ll_x \phi(t, s_g^0, \mu_2 h(\cdot, \tau))$ and both flows belong to $\partial \mathcal{A}$. This in turn implies that the set $\partial \mathcal{A}$ contains comparable points, that is, the set $\partial \mathcal{A}$ is not unordered. We arrive at a contradiction, and hence the interval I is empty and for any τ there exists a unique $\mu_g(\tau)$. This is equivalent to $\mu_g(\cdot)$ being a graph of a function. Using similar arguments, we can show that the inverse mapping $\mu_g^{-1}(\tau)$ is also a graph of a function, which indicates that $\mu_g(\cdot)$ is a decreasing function.

Similarly, we can show that for any μ the minimum value of $\tau_2 - \tau_1$, such that the pairs $(\mu, \tau_1 - \varepsilon) \in \mathcal{S}_g^-, (\mu, \tau_2 + \varepsilon) \in \mathcal{S}_g^+$ for all $\varepsilon > 0$, is equal zero. This readily implies that $\mu_g(\tau) = \nu_g(\tau)$ and completes the proof.

Before we proceed with the proof of Theorem 7 we will need two additional results.

Lemma 10. Let the system $\dot{x} = g(x, 0)$ satisfy Assumption A1 and be monotone on $\mathcal{A}(s_g^0)$, where s_g^0 is a stable steady state and $\mathcal{A}(s_g^0)$ is its domain of attraction. Let x^b and x^l belong to $\mathcal{A}(s_g^0)$. Then all points z such that $x^l \preceq_x z \preceq_x x^b$ belong to $\mathcal{A}(s_g^0)$.

- Elowitz, M. B., Levine, A. J., Siggia, E. D., & Swain, P. S. (2002). Stochastic gene expression in a single cell. *Science Signalling*, 297(5584), 1183.
- Gardner, T., Cantor, C. R., & Collins, J. J. (2000). Construction of a genetic toggle switch in *escherichia coli*. *Nature*, 403, 339–342.
- Gennat, M., & Tibken, B. (2008). Computing guaranteed bounds for uncertain cooperative and monotone nonlinear systems. In *Preprints IFAC world congress* (pp. 4846–4851).
- Jiang, J., Liang, X., & Zhao, X.-Q. (2004). Saddle-point behavior for monotone semiflows and reaction–diffusion models. *Journal of Differential Equations*, 203(2), 313–330.
- Khalil, H. K. (2002). *Nonlinear systems*. Prentice Hall.
- Khalil, A. S., & Collins, J. J. (2010). Synthetic biology: applications come of age. *Nature Reviews Genetics*, 11(5), 367–379.
- Levskaya, A., Weiner, O. D., Lim, W. A., & Voigt, C. A. (2009). Spatiotemporal control of cell signalling using a light-switchable protein interaction. *Nature*, 461, 997–1001.
- Menolascina, F., Di Bernardo, M., & Di Bernardo, D. (2011). Analysis, design and implementation of a novel scheme for in-vivo control of synthetic gene regulatory networks. *Automatica*, 47(6), 1265–1270. Special Issue on Systems Biology.
- Mettetal, J. T., Muzzey, D., Gomez-Urbe, C., & van Oudenaarden, A. (2008). The frequency dependence of osmo-adaptation in *saccharomyces cerevisiae*. *Science*, 319(5862), 482–484.
- Meyer, P.-J., Girard, A., & Witrant, E. (2013). Controllability and invariance of monotone systems for robust ventilation automation in buildings. In *Proc. IEEE conf. decision control* (pp. 1289–1294).
- Miliás-Argeitis, A., Summers, S., Stewart–Ornstein, J., Zuleta, I., Pincus, D., El-Samad, H., & Lygeros, J. (2011). In silico feedback for in vivo regulation of a gene expression circuit. *Nature Biotechnology*, 29(12), 1114–1116.
- Pan, W., Sootla, A., & Stan, G.-B. (2014). Distributed reconstruction of nonlinear networks: An ADMM approach. In *Preprints IFAC world congress. August* (pp. 3208–3213).
- Purnick, P. E. M., & Weiss, R. (2009). The second wave of synthetic biology: from modules to systems. *Nature Reviews Molecular Cell Biology*, 10(6), 410–422.
- Ramdani, N., Meslem, N., & Candau, Y. (2009). A hybrid bounding method for computing an over-approximation for the reachable set of uncertain nonlinear systems. *IEEE Transactions on Automatic Control*, 54(10), 2352–2364.
- Ramdani, N., Meslem, N., & Candau, Y. (2010). Computing reachable sets for uncertain nonlinear monotone systems. *Nonlinear Analysis. Hybrid Systems*, 4(2), 263–278.
- Sontag, E. D. (2007). Monotone and near-monotone biochemical networks. *Systems and Synthetic Biology*, 1(2), 59–87.
- Sootla, A. (2015). On monotonicity and propagation of order properties. In *Proc. Am. control conf. Chicago, Il, June* (pp. 3144–3149).
- Sootla, A., Oyarzún, D., Angeli, D., & Stan, G.-B. (2015). Shaping pulses to control bistable biological systems. In *Proc. Amer. control conf.* (pp. 3138–3143).
- Sootla, A., Strelkova, N., Ernst, D., Barahona, M., & Stan, G.-B. (2013). On reference tracking using reinforcement learning with application to gene regulatory networks. In *Proc. conf. decision control. Florence, Italy, December 10–13* (pp. 4086–4091).
- Sootla, A., Strelkova, N., Ernst, D., Barahona, M., & Stan, G.-B. (2014). Toggling the genetic switch using reinforcement learning. In *Proc. 9th french meeting on planning, decision making and learning. Liège, Belgium, May*.
- Strelkova, N., & Barahona, M. (2010). Switchable genetic oscillator operating in quasi-stable mode. *Journal of the Royal Society Interface*, 7(48), 1071–1082.
- Tipping, M. E. (2001). Sparse Bayesian learning and the relevance vector machine. *Journal of Machine Learning Research*, 1, 211–244.
- Uhlendorf, J., Miermont, A., Delaveau, T., Charvin, G., Fages, F., Bottani, S., & Hersen, P. (2012). Long-term model predictive control of gene expression at the population and single-cell levels. *Proceedings of the National Academy of Sciences*, 109(35), 14271–14276.
- Wilhelm, T. (2009). The smallest chemical reaction system with bistability. *BMC Systems Biology*, 3(1), 90.
- Wipf, D., Nagarajan, S., Platt, J., Koller, D., Singer, Y., & Roweis, S. (2008). A new view of automatic relevance determination. *Advances in Neural Information Processing Systems*, 20, 1625–1632.

- Zwolak, J. W., Tyson, J. J., & Watson, L. T. (2004). Finding all steady state solutions of chemical kinetic models. *Nonlinear Analysis: Real World Applications*, 5(5), 801–814.



Aivar Sootla received his Masters degree in Applied Mathematics from Lomonosov Moscow State University (Russia) and his Ph.D. degree in Control Engineering from Lund University (Sweden). Since 2014 he is an F.R.S-FNRS Research Fellow at University of Liege (Belgium) with the main research focus on control and analysis of monotone systems with biological and biomedical applications.



Diego Oyarzún obtained his Licenciatura and Magister degrees in Electronic Engineering from Universidad Técnica Federico Santa María (Chile, 2006), and his Ph.D. degree from the National University of Ireland, Maynooth (2010). Since 2013 he is a Research Fellow in Biomathematics at Imperial College London, where he develops mathematical methods for the analysis and design of biomolecular networks.



David Angeli is a Reader within the Dept. of Electrical and Electronic Engineering of Imperial College London and Associate Professor at the Dept. of Information Engineering of Florence University (Italy). He is author of more than 70 papers in the areas of Control Engineering, Stability of Nonlinear Systems, Chemical Reaction Networks and Systems Biology. He was nominated IEEE Fellow in 2015 and has served in recent years as Associate Editor of IEEE Trans. On Automatic Control and Automatica.



Guy-Bart Stan is a Reader in Engineering Design for Synthetic Biology and the head of the “Control Engineering Synthetic Biology” group at the Department of Bioengineering of Imperial College London. He is the recipient of the prestigious UK Engineering and Physical Sciences Research Council (EPSRC) Fellowship for Growth in Synthetic Biology, directly supporting his research from February 2015 until January 2020. He received his Ph.D. in Applied Sciences (nonlinear dynamical systems and control) from the University of Liège, Belgium, in March 2005 and subsequently worked as Senior DSP Engineer and R&D coordinator for Philips Applied Technologies, Leuven, Belgium. From January 2006 until December 2009, he worked as Research Associate in the Control Group of the University of Cambridge, first supported by a Marie Curie Intra-European Fellowship and then by the UK EPSRC. He joined the Department of Bioengineering and the Centre for Synthetic Biology and Innovation at Imperial College in December 2009. He has held invited visiting scientist positions at MIT in the Laboratory for Information and Decision Systems (July–Sep 2008) and the Department of Mechanical Engineering (Aug–Sep 2015). His current research focus is on the study of the core engineering design principles of complex dynamical systems, including biological systems and complex networks, and on the development of mathematical modelling, analysis, and systems and control engineering methods for such systems. He is author of over 70 peer-reviewed papers and 1 book, and co-editor of a 2 volumes book on the use of rigorous systems and control engineering methods for solving important problems in systems biology, synthetic biology and complex physical systems.